AIAA JOURNAL
Vol. 44, No. 6, June 2006

Unsteady Aerodynamics Analysis of Flat Plates in Pitch Oscillation

Cheolheui Han* and Jinsoo Cho†
Hanyang University, Seoul 133-791, Republic of Korea

The fluid propulsion mechanism of two oscillating flat plates is studied numerically using a discrete vortex method. Presently, the flat plates are assumed to be rigid. To analyze the closely coupled aerodynamic interference between the plates, a core addition scheme and a vortex core model are combined. The calculated wake pattern for a flat plate in heaving oscillation motion is compared using flow visualization. The effect of the wake shapes on the aerodynamic characteristics of the flat plate in pitching oscillation is investigated. The velocity contours at a certain distance behind the flat plates in pitching oscillations with several frequencies are plotted to investigate the possible thrust generation mechanism. The aerodynamic characteristics of the flat plates in pitching oscillation are also investigated.

Nomenclature

A_{ij}	=	normal component of velocity induced at control point i by unit circulation at node j
c	=	chord length, m
c_d	=	drag coefficient, $D/0.5\rho U_\infty^2 c$
c_t	=	thrust coefficient, $T/0.5\rho U_\infty^2 c$
D	=	drag force, N
d	=	distance between leading edges of plates, m
h	=	heaving oscillation amplitude, m
k	=	reduced frequency, $\omega c/U_\infty$, rad
N	=	number of nodes on flat plate
$\boldsymbol{n}_i$	=	unit normal vector at control point i
p	=	pitching oscillation amplitude, rad
Q_i	=	normal velocity induced at control point i by unit circulation at trailing edge
r_c	=	vortex core radius, m
T	=	thrust force, N
t	=	time, s
U_∞	=	freestream velocity component in x direction, m/s
X, Y	=	ground-fixed coordinates
x, y	=	body-fixed coordinates
α	=	angle of attack, deg or rad
Γ	=	circulation of point vortex
Δl	=	panel length, m
Δt	=	time step, s
θ	=	pitch angle, rad
λ	=	wake wavelength, m
ρ	=	freestream density, kg/m^3
Φ	=	velocity potential
ω_h	=	heaving oscillation frequency, rad/s
ω_p	=	pitching oscillation frequency, rad/s

I. Introduction

UNLIKE large birds, whose flapping is restricted to limited operations such as takeoff and landing, small birds and insects use the flapping-wing mechanism to generate lift to overcome their weight. This mechanism has the advantage that when the size decreases, flapping-wing flight is much more efficient than fixed-wing flight.[1] With the rapid progress in microelectromechanical systems, roboticists began to think small.[2] Research and development for machines that achieve insect-like or birdlike flight performance, initiated a century ago,[3] is now being further refined in the development of micro air vehicles (MAVs).[1]

Among others, utilizing a piezoelectric foil as a propulsive device for MAVs might be promising.[4] The piezoelectric foil is a very thin electromechanical converter that can convert electrical to mechanical energy and vice versa. The high strength and sensitivity of the material allows the use in an extreme dynamic and frequency range, from 10^{-8} to 10^5 N/cm^2 in the direction of thickness and at frequencies between 0.001 Hz and several gigahertz (Ref. 5). Thus, the piezoelectric foil technique allows the design of extremely flexible actuators.

Jones et al.[6] studied wake structures behind a flapping airfoil and the ability of a sinusoidally plunging airfoil to produce thrust (known as the Knoller–Betz effect) experimentally and numerically. They demonstrated that the formation and evolution of unsteady wakes is fundamentally an inviscid phenomenon over a broad range of Strouhal numbers. Jones and Platzer[7–9] obtained flow solutions about several airfoil configurations and predicted marginal improvement of thrust in the four-airfoil systems comparing with two airfoils. Akiyama et al.[10] studied the flowfield around vibrating elastic plates. Two piezopolymer plates were actuated in the same phase and in the opposite phase. They observed that flowfields around the vibrating plates created counter-rotating vortices and that the pressure distribution around the plates produced the driving propulsion flow from the leading edge to the trailing edge. Despite a wide spectrum of engineering applications using vibrating elastic plates, not much has been studied on the fluid propulsion mechanism.

Thus, the purpose of this paper is to investigate the flow characteristics of two oscillating plates and to identify the fluid propulsion mechanism. As a first stage to the unsteady aerodynamic analysis of vibrating elastic plates, a configuration for two airfoil systems is investigated by assuming that the flat plates are rigid and oscillating. To predict accurately the closely coupled interacting wakes between plates, a core addition scheme[11] and a vortex core model[12] are combined.[13] A calculated wake pattern for a flat plate in heaving oscillation motion is compared with the experimental flow visualization.[14] The velocity contours at a certain distance behind the oscillating flat plates with several frequencies are plotted to investigate the possible thrust generation mechanism.

II. Method of Analysis

To treat the unsteady motions of flat plates moving through the air, two coordinate systems are used (Fig. 1). One is a body-fixed coordinate system (x, y). The other is the inertial frame of reference

Presented as Paper 2003-3674 at the 21st Applied Aerodynamics Conference, Orlando, FL, 23–27 June 2003; received 2 February 2004; accepted for publication 13 December 2005.

*Professor Lecturer, School of Mechanical Engineering. Member AIAA.
†Professor, School of Mechanical Engineering. Senior Member AIAA.

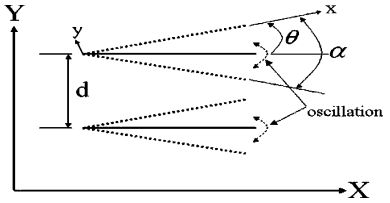

Fig. 1 Coordinate systems: x, y, body-fixed frame of reference; X, Y, stationary inertial frame of reference; Θ, pitch angle; α, angle of attack; and d, distance between leading edge of the plates.

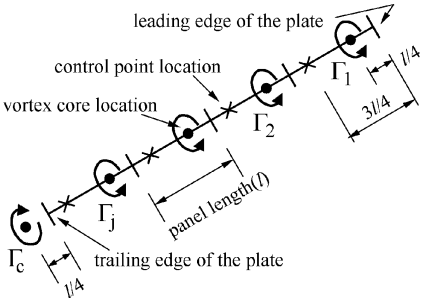

Fig. 2 Discretization of flat plate.

(X, Y). The flow is assumed to be inviscid, incompressible, and irrotational over the entire flowfield, excluding the flat plates' solid boundaries and their wakes. A velocity potential $\Phi(X, Y)$ can be defined in the inertial frame, and the continuity equation becomes the Laplace equation. Mass is conserved regardless of the coordinate systems. Therefore, in x, y coordinates,

$$\nabla^2 \Phi = 0 \tag{1}$$

A flat plate is discretized into $(N-1)$ equal length panel elements. The vorticity on each element is considered to be uniform. The vorticity of uniform strength on each element is replaced by a point vortex of strength Γ_j located at a distance equal to one-quarter of the element length behind its leading edge, as shown in Fig. 2. The wake is represented by free vortices that deform freely by the assumption of a force-free position during the simulation. These free vortices are connected to the bound vortices at the trailing edge of the plate through the Kutta condition. The strengths of the elementary solutions are obtained by enforcing boundary conditions as follows:

1) The flow disturbance, due to the plate's motion through the fluid, should vanish far from the plates. This boundary condition can be satisfied automatically by using the discrete vortices as the singularity distributions.

2) There is zero normal flow across the plates' solid boundaries. The continuity equation (1) does not directly include time-dependent terms. Time dependency is introduced through the modification of zero normal flow on a solid surface and the use of the unsteady Bernoulli equation. If the kinematic velocity $\boldsymbol{v}$ is given as

$$\boldsymbol{v} = -[\boldsymbol{V}_0 + \boldsymbol{v}_{\text{rel}} + \boldsymbol{\Omega} \times \boldsymbol{r}] \tag{2}$$

where $\boldsymbol{V}_0$ is the velocity of the body-fixed system's origin, $\boldsymbol{r} = (x, y, z)$ is the position vector, $\boldsymbol{\Omega}$ is the rate of rotation of the body's frame of reference, and $\boldsymbol{v}_{\text{rel}}$ is the additional relative motion within the (x, y, z) system. The zero-velocity normal to a solid surface boundary in the body-fixed frame becomes (in x, y coordinates)

$$(\nabla \Phi - \boldsymbol{V}_0 - \boldsymbol{v}_{\text{rel}} - \boldsymbol{\Omega} \times \boldsymbol{r}) \cdot \boldsymbol{n} = 0 \tag{3}$$

where $\boldsymbol{n}$ is normal to the body's surface in terms of the body coordinates (x, y). The plate is considered rigid, hence, $\boldsymbol{v}_{\text{rel}}$ is equal to zero. Also, $\boldsymbol{\Omega}$ is assumed to be zero. Fulfilling the boundary condition on the surface requires that, at each collocation point, the normal velocity component will vanish, and we can write Eq. (3) as

$$\sum_{j=1}^{N-1} a_{ij}\Gamma_j - q_i\Gamma_c = (\boldsymbol{V}_0 - \boldsymbol{V}_{wi}) \cdot \boldsymbol{n}_i \tag{4}$$

on the plate for $i = 1, 2, \ldots, N-1$, where the influence matrix element a_{ij} represents the normal velocity component at a control point i by the point vortex (having a unit circulation) at the panel element j and its image. The elements a_{ij} are functions of geometry. Γ_j is the unknown circulation of the point vortex representing the vorticity of the panel element j. Here, q_i represents the normal velocity component induced at control point i by the starting vortex and its image. $\boldsymbol{V}_{wi}$ is the velocity induced by the wake vortices and their images whose positions and circulations are known. At the beginning, $\boldsymbol{V}_{wi}$ is zero.[15] The calculation begins at $t = \Delta t$ and the wake at this moment consists of a single vortex Γ_c. Following Mook et al.,[11] we simulate the starting vortex by placing it at a point $\frac{1}{4}\,l$ behind an airfoil trailing edge (Fig. 2).

3) The use of the Kelvin condition that the circulation around a fluid curve enclosing the plates and their wakes is conserved will supply an additional equation,

$$\sum_{j=1}^{N-1} \Gamma_j - \Gamma_c = \sum_{j=1}^{\text{NT}-1} \Gamma_{\text{wake}} \tag{5}$$

where the number of time steps (NT) is used. Γ_{wake} is the circulation of a wake core at node k, which is zero at the start of motion. The wake is created as a result of shedding and convecting the starting vortex at each time step.

4) The unsteady Kutta condition at the trailing edge of a plate is satisfied by shedding the vorticity generated at the trailing of a plate at the local fluid particle velocity.[15]

5) Continuous pressure across the wake is fulfilled with convecting wakes downstream at the local fluid particle velocity.

To solve Eqs. (4) and (5), an initial condition describing the position of the wake and its vorticity must be prescribed. At each time step, a newly shed starting vortex is fixed at a point $\frac{1}{4}\,l$ behind a plate's trailing edge as required by the unsteady Kutta condition. All of the circulation strengths are determined including the effects of their images by Gauss elimination. At the end of each time step, the shed vortex is convected downstream to its new position at the local fluid particle velocity. The procedure is repeated for any desired number of time steps.

A. Wake Roll Up

Because the wake is force free, each vortex representing the wake must move with the local flow velocity. The local flow velocity is the result of the velocity components induced by the wake and the plate. It is measured in the inertial frame of reference (X, Y). To achieve the vortex wake rollup at each time, the induced velocity $(u, v)_i$ at each vortex wake point i is calculated, and then the vortex elements are moved by an Euler convection scheme. In the regions where vortex cores are separating, leaving large gaps and beginning to reassemble, the unequal spacing between the cores can lead to numerical instabilities.[11] The core addition scheme imitates the elongated region of the vorticity in the actual flow. If the distance between two successively shedding cores is separated by more than a prescribed critical length, a new core is located at the midpoint of the line segment connecting them. This new core has one-third the sum of circulations around the two original cores. The circulations around the two original cores are reduced by a factor of two-thirds. The velocity within the core v_j with a core radius r_c at time t is

$$v_j = (\Gamma_j/2\pi r)\{1 - \exp[-1.25643(r/r_{cj})^2]\} \tag{6}$$

where Γ_j is a strength of a vortex and r is the distance between the origin of the vortex core and the point in space.[12] Outside the core region, the induced velocity can be taken as that of a free vortex of strength Γ_j.

B. Computation of Aerodynamic Loads

In the body-fixed frame, thrust (or drag) is calculated using the momentum conservation theorem

$$T(\text{or } D) = \rho \int_{-\infty}^{\infty} V(y)[V(y) - U_\infty]\,\mathrm{d}y \tag{7}$$

where $V(y)$ is the velocity profile at the cross section behind a chord length from the plate's trailing edge and U_∞ is the freestream velocity.

III. Results and Discussion

A. Single Flat Plate

In Fig. 3, a calculated wake pattern for a flat plate in heaving oscillation motion is compared with the flow visualization by Bratt.[14] The use of vortex core modeling[12] and the core addition scheme[11] can be validated by comparing the results with the time-step reduction scheme.[13] In Fig. 3, the flat plate is undergoing heave oscillations with $\alpha = 0$ deg, $h = 0.019$, and $\omega_h c/2U = 8.5$. Both use of the core addition scheme with $L_{cr} = 3.0 \times \Delta t$ and the vortex core model with $r_c = 0.03c$ eliminate the unequal spacing between the cores while reducing the computing time. In Fig. 3, the computed result shows good agreement with the other numerical result[16] and flow visualization.[14]

Figure 4 shows calculated wake shapes for a flat plate in pitching oscillation, $\omega_p \times c/U_\infty = 13.38$, $\Delta t = 0.01$, $r_c = 0.03c$, and $p = 0.02$. Figure 4a shows an accurately predicted wake shape, whereas Fig. 4b presents an inaccurately calculated wake shape. The result in Fig. 4b is obtained without using the core addition scheme.

a) Flow visualization

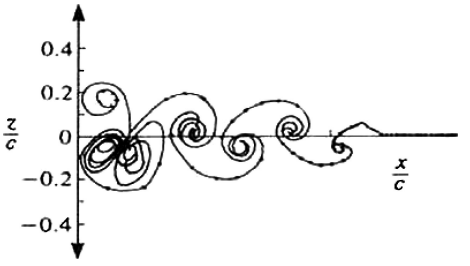

b) Katz[15]

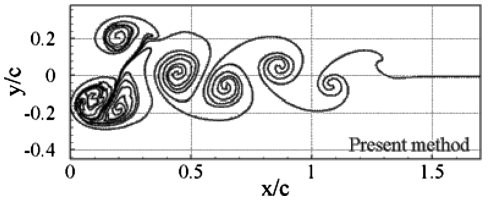

c) Present method

Fig. 3 Wake patterns behind flat plate undergoing heave oscillation.

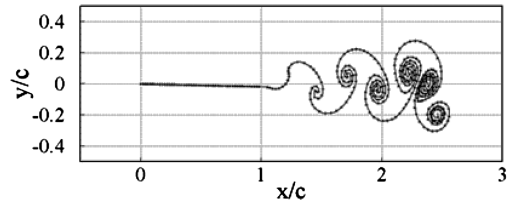

a) Accurate

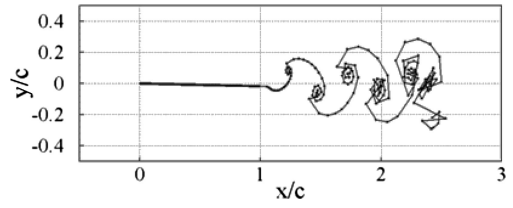

b) Inaccurate

Fig. 4 Predicted wake shapes behind flat plate undergoing heave oscillation: $\Delta t = 0.01$, $r_c = 0.03c$, $p = 0.02$, and $\omega_p \times c/U_\infty = 13.38$.

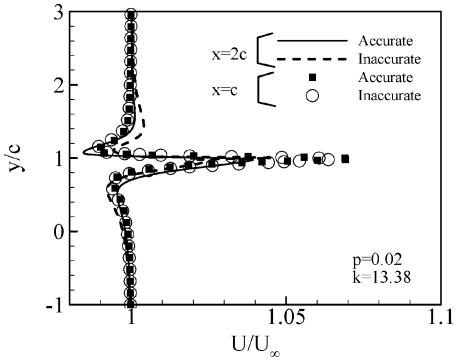

Fig. 5 Effect of accurate wake simulation for velocity profile calculations at cross section at chord length downstream of plate.

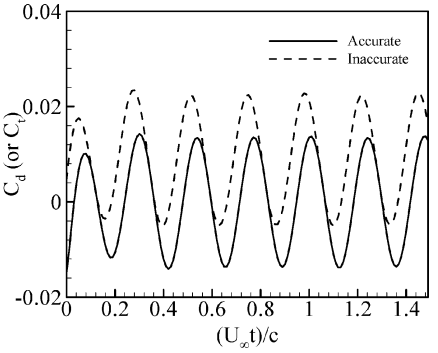

Fig. 6 Effect of accurate wake simulation in thrust coefficient prediction: accurate $c_t = 4.06 \times 10^{-3}$ and inaccurate $c_t = 2.55 \times 10^{-3}$.

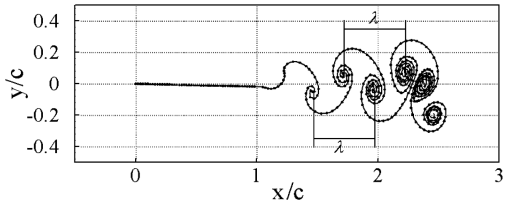

Fig. 7 Definition of wake wavelength.

Figures 5 and 6 show the effect of an accurate wake shape simulation on predicting the aerodynamic and flow characteristics of a flat plate oscillating in pitch. In Fig. 5, velocity profiles are plotted at the cross section, just behind the trailing edge and a chord length downstream of the plate's trailing edge. As shown in Fig. 5, the wake simulation has very little effect on calculating the velocity profiles at the trailing edge. However, it becomes important when the calculation of velocity profiles is performed at a distance from the trailing edge. Figure 6 shows that the predicted thrust coefficients with an accurate wake shape are larger than those with an incorrect wake shape.

Qualitative validation of the present method is done by comparing calculated wake wavelengths behind a heaving oscillating flat plate with those behind a NACA 0012 airfoil by a panel method[7] and flow visualization.[7] Figure 7 shows a definition of the wavelength of the vortex street behind an oscillating flat plate. In Fig. 8, the wake wavelengths calculated by the present method are compared with those by a panel method and experimental data.[7] The wavelengths are plotted as a function of heaving amplitude for $k = 3.00$, $k = 6.83$, and $k = 12.32$. The airfoil thickness effect on the propulsive efficiency of the flat plate in heaving oscillation was investigated by Jones and Platzer.[7] The airfoil thickness has very little effect on the aerodynamic characteristics of plunging airfoils, whereas it affects the thrust production for pitching airfoils. It can be seen in Figs. 8 and 9 that, although the present result is for a flat plate, whereas Jones and Platzer[7] used the NACA0012 airfoil, the results for heaving oscillation agree well.

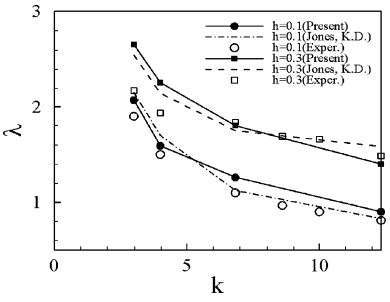

Fig. 8 Wake wavelength vs reduced frequency.

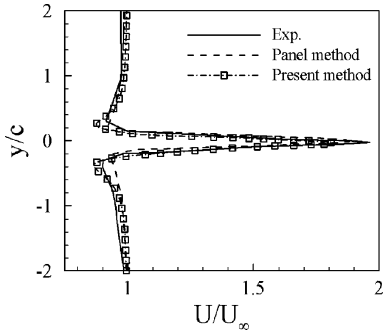

Fig. 9 Nondimensionalized velocity profiles 0.4*c* downstream of trailing edge of airfoil.

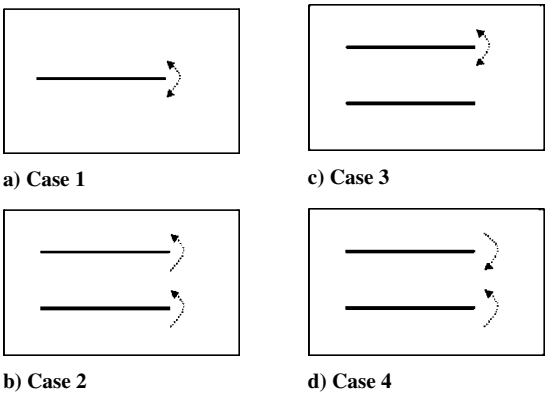

Fig. 10 Nomenclature for study on propulsion mechanism of two flat plates in pitching oscillations.

In Fig. 9, the velocity profile calculated by the present method is compared with those by the panel method and the experiment. The velocity profile by the present method is calculated at the cross section 0.4*c* downstream of the trailing edge of a flat plate undergoing heave oscillations with $h = 0.04$ and $k = 15.0$. It can be deduced from Fig. 9 that the velocity profile calculated by the present method shows good agreement with that by the panel method and experimental data.

B. Two-Flat-Plate Systems

Figure 10 shows the nomenclature for the study on the propulsion mechanism for two flat plates in pitching oscillations. Case 1 is for a single flat plate. Cases 2–4 are for two flat plates. In case 2, both plates are undergoing a pitch oscillation in phase. In case 3, only the upper plate is oscillating, whereas the lower plate is stationary. Contrary to case 2, the plates in case 4 are oscillating in the opposite phase.

Figure 11 shows wake patterns behind the two flat plates in pitching oscillations. The wake patterns are calculated for $\alpha_0 = 0$ deg, $p = 0.1$, $U_\infty/c = 1.0$, $\Delta t = 0.01$, $\omega_p \times c/U_\infty = 5.0$, $d = 0.25c$, $L_{\text{critical}} = 4.0 \times \Delta t$, and $r_c = 0.04c$. As shown in Fig. 11b, the wake vortices from the oscillating plates in phase are convected in phase. When only an upper plate is oscillating and the other lower plate is moving forward without oscillation (Fig. 11c), the starting vortex is also generated behind the lower plate by the aerodynamic interaction with the upper plate. This starting vortex interacts with vortices from the upper plate. In Fig. 11d, the wake vortices behind plates undergoing a pitch oscillation in the opposite phase are shown to be symmetric with each other.[17]

Figure 12 shows nondimensionalized velocity profiles at one wake wavelength downstream of the trailing edge of the plates.

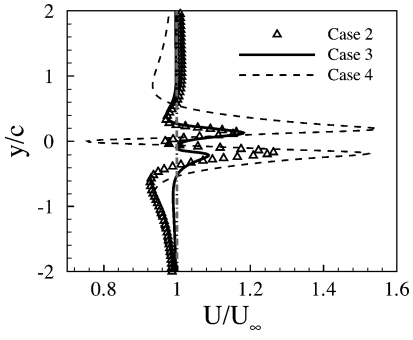

Fig. 12 Nondimensionalized velocity profiles at chord length downstream of trailing edge of plates: $p = 0.1$ and $k = 6.26$.

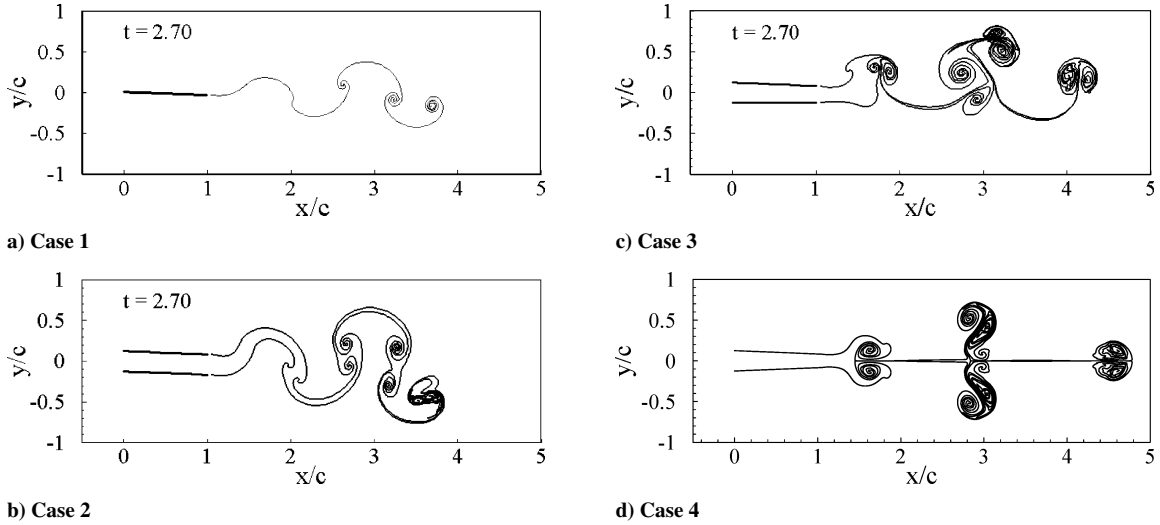

Fig. 11 Wake patterns behind two flat plates in pitching oscillations.

Two-plate systems produce two peaks larger than one in the nondimensionalized velocity profiles, whereas one plate generates one peak in the profile. The peaks in case 4 have larger values than cases 2 and 3. Thus, it can be assumed that the case 4 is more propulsive than the other cases.

This assumption is clearly verified in Fig. 13, where the time-averaged thrust coefficients are plotted as a function of the pitching reduced frequency k. For all frequency ranges, the plates undergoing a pitch oscillation out of phase produce larger propulsive forces than other cases. For frequencies less than seven, case 3 produces larger thrust force than case 2.

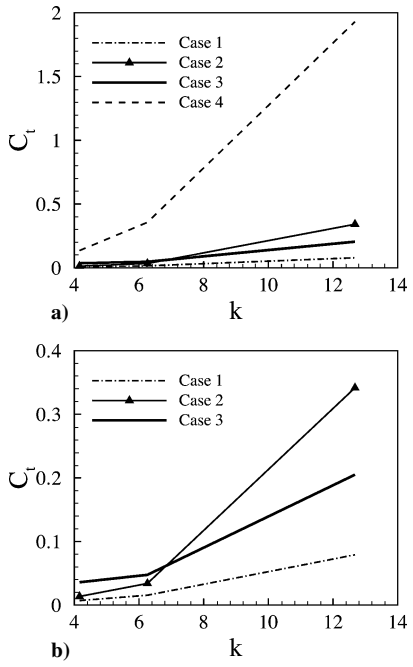

Fig. 13 Time averaged thrust coefficients vs frequency, $p = 0.088$.

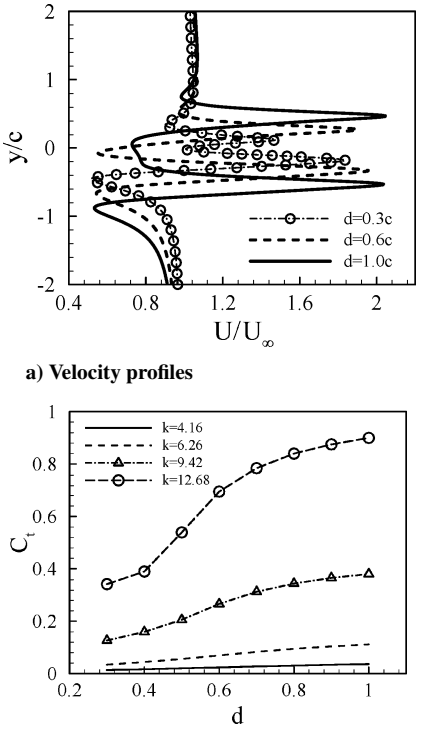

Fig. 14 Effect of distance between leading edges of plates in pitching oscillation with mode of case 2: $p = 0.075$ and $k = 12.68$.

Figure 14 shows the effect of the vertical distance between the leading edges of the plates on the flow and aerodynamic characteristics of the pitching plates in phase (case 2). In Fig. 14a, the time-averaged nondimensionalized velocity profiles behind the oscillating plates with $p = 0.075$ and $k = 12.68$ are plotted when the distances are $0.1c$, $0.3c$, and $1.0c$. In Fig. 14b, time-averaged thrust coefficients are also plotted as a function of frequency. (The pitching amplitude is fixed as $p = 0.088$.) In Fig. 14a, the peaks larger

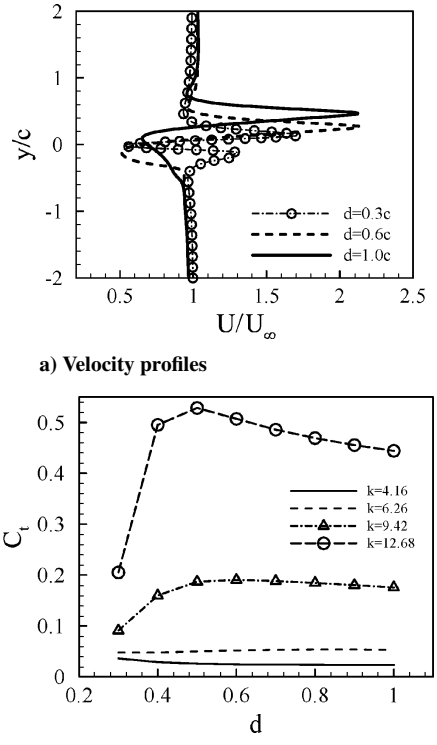

Fig. 15 Effect of distance between leading edges of plates in pitching oscillation with mode of case 3: $p = 0.075$ and $k = 12.68$.

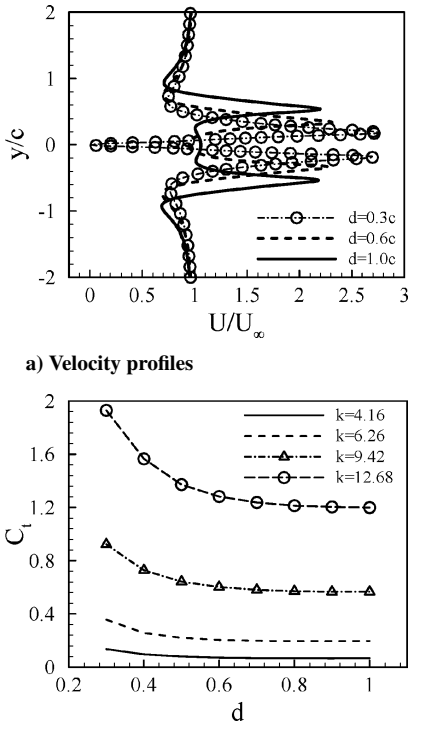

Fig. 16 Effect of distance between leading edges of plates in pitching oscillation with mode of case 4: $p = 0.075$ and $k = 12.68$.

than one are augmented as the distances between the plates increase. The thrust coefficients shown in Fig. 14b are also increased when the plates are separated with a large distance.

Figure 15a shows the variation of velocity profiles and thrust coefficients for case 3 when the distance between the leading edges of the plates is increased. When the distance is large and $k = 12.68$, the lower plate does not produce flows with velocities larger than freestream. In Fig. 15b, the thrust coefficient of the plates decreases when the distance is larger than $0.5c$ and $k = 12.68$.

In Fig. 16a, the time-averaged nondimensionalized velocity profiles behind the oscillating plates with $p = 0.075$ and $k = 12.68$ are plotted when the distances are $0.3c$, $0.6c$, and $1.0c$. As shown in Fig. 15a, the peaks in the velocity profiles decrease when the distance increases. The time-averaged thrust coefficients plotted in Fig. 16b show the decrease in the values of thrust coefficient as the distance increases.

IV. Conclusions

This study demonstrates the possible fluid propulsion mechanism of two oscillating flat plates. A calculated wake pattern for a flat plate in heaving oscillation motion is compared with the flow visualization. The effect of accuracy in the representation of rolled-up wake shapes is investigated for a single pitching plate. This study shows that inaccurately represented wake vortices cause inaccurate results in predicting the force coefficients. The aerodynamic characteristics of the flat plates in pitching oscillation are investigated. The flat plates oscillating out of phase produce larger thrust than the other plates. For all frequency ranges, the distance between the plates of case 2 has an effect of increasing thrust, whereas, in case 4, the distance decreases thrust. In case 3, the thrust increases when the distance and the frequency are larger than $0.5c$ and 6.26, respectively.

Acknowledgment

This work was supported by a Korea Research Foundation Grant funded by the Government of the Republic of Korea (Ministry of Education and Human Resources Development, Basic Research Promotion Fund KRF-2005-206-D00007).

References

[1]Mueller, T. J., *Fixed and Flapping Wing Aerodynamics for Micro Air Vehicle Applications,* AIAA, Reston, VA, 2001, Chap. 77.

[2]Yan, J., Wood, R., Avandhanula, S., Sitti, R., and Fearing, R. S., "Towards Flapping Wing Control for a Micromechanical Flying Insect," *IEEE International Conference on Robotics and Automation*, IEEE Robotics and Automation Society, Seoul, Republic of Korea, 2001, pp. 3901–3908.

[3]Lighthill, M. J., *Collected Papers of Sir James Lighthill*, edited by M. Yousuff Hussaini, Vol. 4, Oxford Univ. Press, New York, 1997, Chap. 1.

[4]Sitti, M., Campolo, D., Yan, J., Fearing, R. S., Su, T., Taylor, D., and Sands, T., "Development of PZT and PZN-PT Based Unimorph Actuators for Micromechanical Flapping Mechanisms," *IEEE International Conference on Robotics and Automation*, IEEE Robotics and Automation Society, Seoul, Republic of Korea, 2001, pp. 3839–3846.

[5]"Piezoelectric Foil Sensors and Actuators," URL: http://w2.nasatech.com/ITB/test_and_control.html [cited 10 Feb. 2003].

[6]Jones, K. D., Dohring, C. M., and Platzer, M. F., "Wake Structures Behind Plunging Airfoils: A Comparison of Numerical and Experimental Results," AIAA Paper 96-0078, Jan. 1996.

[7]Jones, K. D., and Platzer, M. F., "Flapping-Wing Propulsion for a Micro Air Vehicle," AIAA Paper 2000-0897, Jan. 2000.

[8]Jones, K. D., and Platzer, M. F., "Numerical Computation of Flapping-Wing Propulsion and Power Extraction," AIAA Paper 97-0826, Jan. 1997.

[9]Jones, K. D., and Platzer, M. F., "An Experimental and Numerical Investigation of Flapping-Wing Propulsion," AIAA Paper 99-0995, Jan. 1999.

[10]Akiyama, M., Takato, K., Tsutsui, T., Sugiyama, H., and Ninimiya, N., "Flow Around Vibrating Elastic Plates," *Proceedings of 6th Asian Symposium on Visualization*, Pusan, Republic of Korea, 2001, pp. 73–75.

[11]Mook, D. T., Roy, S., Choksi, G., and Dong, B., "Numerical Simulation of the Unsteady Wake Behind an Airfoil," *Journal of Aircraft*, Vol. 26, No. 6, 1989, pp. 509–514.

[12]Ling, G. C., Bearman, P. W., and Graham, J. M. R., "A Further Simulation of Starting Flow Around a Flat Plate by a Discrete Vortex Model," *Internal Seminar on Engineering Applications of the Surface and Cloud Vorticity Methods*, Vol. 51, No. 14, 1986, pp. 118–138.

[13]Han, C., Yoon, Y., and Cho, J., "Unsteady Aerodynamics Analysis of Tandem Flat Plates in Ground Effect," *Journal of Aircraft*, Vol. 39, No. 6, 2002, pp. 1028–1034.

[14]Bratt, J. B., "Flow Patterns in the Wake of an Oscillating Airfoil," Aeronautical Research Council, R&M 2773, March 1953.

[15]Katz, J., and Plotkin, A., *Low-Speed Aerodynamics*, Cambridge Univ. Press, Cambridge, England, U.K., 2001, Chap. 13.

[16]Katz, J., and Weihs, D., "Behavior of Vortex Wakes from Oscillating Airfoils," *Journal of Aircraft*, Vol. 15, No. 12, 1978, pp. 861–863.

[17]Jones, K. D., Castro, B. M., Mahmoud, O., and Platzer, M. F., "A Numerical and Experimental Investigation of Flapping-Wing Propulsion in Ground Effect," AIAA Paper 2002-0866, Jan. 2002.

E. Livne
Associate Editor